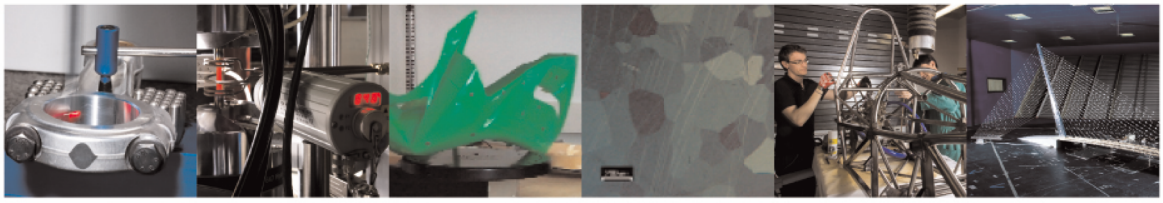

# Wind tunnel pressure data analysis for peak cladding load estimation on a high-rise building

Giulia Pomaranzi, Luca Amerio, Paolo Schito, Giacomo Lamberti, Catherine Gorlé, Alberto Zasso

This is a post-peer-review, pre-copyedit version of an article published in *Journal of Wind Engineering and Industrial Aerodynamics*. The final authenticated version is available online at: http://dx.doi.org/10.1016/j.jweia.2021.104855



DIPARTIMENTO DI MECCANICA ■ POLITECNICO DI MILANO
via G. La Masa, 1 ■ 20156 Milano ■ EMAIL (PEC): pecmecc@cert.polimi.it
http://www.mecc.polimi.it
Rev. 0

# Wind tunnel pressure data analysis for peak cladding load estimation on a high-rise building

Giulia Pomaranzi[a,*], Luca Amerio[b], Paolo Schito[a], Giacomo Lamberti[c], Catherine Gorlé[c], Alberto Zasso[a]

[a]*Politecnico di Milano, Via G. La Masa 1, 20156, Milan, Italy*
[b]*Advanced Technology + Research group, ARUP, UK*
[c]*Stanford University, Y2E2 Building, 473 Via Ortega, Stanford, CA, 94305*

## Abstract

A correct evaluation of wind loads on high-rise building cladding panels is essential to ensure safety while avoiding costly over-design. The estimation of peak design loads from wind tunnel tests requires post-processing pressure time histories to remove small-scale fluctuations that do not significantly affect the total load on cladding elements. This post-processing commonly employs a low pass filter with a time-scale that is linearly proportional to the ratio of a reference length scale and velocity. The objective of this study is to analyze the equivalence between the moving-average filter and the spatial averaging procedure, focusing on panels near the top corners and edges of a high-rise building. The real area-averaged pressure is calculated using high-resolution pressure measurements and compared to estimates obtained from moving-average filters with a range of time-scales. The error is within $\pm 1$ $C_p$ for most pressure tap locations and panels analyzed, although some locations near the top edge result in overestimates of the peak suction up to 3 $C_p$. The optimal value of the proportionality coefficient defining the filter time-scale is shown to be dependent on both pressure tap location and panel size, suggesting that accurate estimates of area-averaged pressures based on single-point measurements require more advanced post-processing techniques.

*Keywords:* Wind Tunnel Tests, Pressure Measurements, Pressure Peak, Cladding Load, TVL

## 1. Introduction

Recent trends in architecture indicate an increase in the adoption of large glazed panels to cover building façades. In many cases, the governing load for the design of these façades is represented by wind pressure, making the calculation of the wind loads on façade elements a crucial issue. Accurate estimates of these loads are not only relevant from a user safety point of view, but also from an economic point of view: the cladding system can account for up to 25% of the total building cost [1]. In current engineering design, one of the possible ways to estimate the wind design pressure is the application of building codes. Code values are based on wind tunnel test results, and defined to be safely applicable to a wide array of building shapes. As a result, they often provide overly conservative estimates. Wind tunnel tests offer an alternative approach to obtain more accurate results, in particular for high-rise or unusually shaped buildings. These

*Corresponding author
*Email addresses:* giulia.pomaranzi@polimi.it (Giulia Pomaranzi), luca.amerio@arup.com (Luca Amerio), paolo.schito@polimi.it (Paolo Schito), giacomol@stanford.edu (Giacomo Lamberti), gorle@stanford.edu (Catherine Gorlé), alberto.zasso@polimi.it (Alberto Zasso)

tests provide a more detailed understanding of the exact pressure field around the building and avoid costly over-design.

The final purpose of a wind tunnel test is the assessment of the design load to be provided to the façade designer. This design load has to represent the maximum correlated pressure over the panel surface area (usually on the order of 5-10 $m^2$). In principle, its value can be calculated directly from integration of the pressure distribution over the area of interest. However, an accurate measurement of this pressure distribution would require a very dense distribution of pressure sensors that is unattainable in practice. For example, considering a high-rise building facade of 50 m x 100 m covered with panels of 3 m x 3 m, $\tilde{5}50$ panels would be required to cover this single facade. Even just placing one pressure tap at the center of each panel would not be possible in most wind tunnels. Current practice is to distribute the available number of pressure taps over the model surface, paying special attention to the edges and corners. The resulting pressure tap resolution is on the order of one pressure tap every 10 $m^2$ or more. While this resolution is sufficient when the quantities of interest are the global loads acting on the structure, it results in highly under-resolved measurements of the spatial variability of the pressure field when the cladding loads are to be estimated. At the same time, the high temporal sampling frequency employed in wind tunnel measurements can capture pressure peaks of very short duration. These short-lived pressure peaks are typically characterized by negligible spatial scales compared to the size of a cladding element, indicating they might not be relevant for cladding design [2]. Hence, high-frequency fluctuations that are assumed to not be representative of the total load acting on the panel are usually removed *a posteriori*.

A practical approach for estimating the *real* area-averaged pressure acting on an area of interest is to assume that the duration of the peak pressure events is proportional to their spatial extent. This concept of proportionality was first proposed by Lawson [3, 4] to address the fact that at that time most pressure tap measurements were unrelated in time due to limited availability of pressure transducers. Based on full-scale pressure measurements performed by Newberry et al. [5] on Royex House, a high-rise building in London, Lawson suggested relating the averaging time $\tau$ to the pressure signal's spatial correlation, specifying $\tau$ as proportional to the ratio between the reference length $L$ of the area of interest and the reference velocity $V$:

$$\tau = \frac{K \cdot L}{V}. \tag{1}$$

In this equation, hereafter referred to as the TVL equation, $K$ is a constant representing the exponential decay factor in the spatial coherence function of the pressure signal, with the reduced frequency (computed as $fV/L$) as independent variable. As such, the $\tau$ value computed through Eq.1 represents the load duration, or equivalent time averaging, for which pressure fluctuations are considered to act simultaneously on a surface characterised by a reference length $L$. The full-scale measurements on the windward face of the Royex House indicated $K = 4.5$. In 1997, Holmes [6] revisited the TVL equation, pointing out that the correlation of the pressure between two points does not provide a measure of the reduction in total load over an area; the total load should be obtained from multiplying the spectral density of a fluctuating point by the local *"aerodynamic admittance"* function [7]. This function can vary from point to point and for different wind directions, depending on the local flow regime. An experimental evaluation of the admittance function would require a spatially-dense distribution of taps, similar to the resolution required to measure the area-averaged pressure distribution itself. Instead, Holmes analytically derived an admittance function based on the assumption of an exponential spatial correlation function. He translated this admittance function into a moving average filter by matching their half-power frequencies, which suggested $\tau = 1.0\ \frac{L}{V}$. The resulting moving average filter closely resembled the measured admittance function on Royex house, but this equation is likely to vary considerably for facades other than the windward one [6, 8].

The possibility to account for the filtering effect of the area averaging through a very simple expression

is the main reason of the popularity of the TVL formula for cladding design, even if its basic assumption of proportionality between the duration and spatial extent of the pressure peaks has not been extensively tested. Recently, Li et al. [9] presented an evaluation of the TVL theory on a 40 m high building roof, focusing on large-scale cladding using an average resolution of 1 pressure tap per 100 $m^2$. The results indicate that the value of K varies as a function of the position on the roof, although this conclusion should be further verified for small-scale cladding. Wacker et al. [10]similarly demonstrated that leading edge roof tiles in oblique wind flow revealed significantly reduced spatial correlations that can lead to a reduction of the dynamic wind load. They also considered two cladding panels on a high-rise building and concluded that the pressure signal measured at the centre tap of the panel was representative of the wind load on the total element. However, the panels were located in regions of attached flow, and the temporal resolution of the measurements was much lower than today's standard practice, such that short-lived peak events might not have been resolved. The reduction in spatial correlation observed on the roofs in both studies is attributed to small-scale peak pressure events occurring just downstream of the leading edge of flat (or nearly-flat) roofs. These events have been extensively studied using wind tunnel tests, in particular on low-rise buildings [11, 12, 13, 14, 15]. However, it remains to be investigated whether these peak events, and the related decrease in spatial correlation, could occur in other regions of separated flow, in particular near the corners and edges of high-rise building facades.

The objective of the present paper is twofold. First, we aim to provide a detailed analysis of the equivalence between the use of a moving-average filter in the time domain and the spatial averaging procedure, including an evaluation of the optimal values of $K$ in the TVL equation. Second, we aim to evaluate the potential of an alternative approach to estimate the area-averaged pressure, using pneumatic averaging over a few pressure taps distributed on a panel. The analysis focuses on locations that are critical for cladding design, i.e. panels near the top corners and lateral edges of a high-rise building façade. Wind tunnel pressure measurements in these locations are available from an experimental campaign performed at the Politecnico di Milano wind tunnel; this data was first presented by Amerio et al. [16] and has been compared and validated against a twin experiment in Florida International University's Wall of Wind (WoW) facility [17]. In these experiments, a high-rise building model was instrumented with 448 pressure taps, placed with a very high resolution in two areas of a lateral facade: one located at the top corner, and one located near the edge at half the building height. The resolution of the pressure measurements on these tiles is sufficiently high to support an accurate calculation of the *real* area-averaged pressure, allowing comparison to the value obtained using a moving-average filter based on the TVL equation, or to the value obtained from the pneumatic averaging over a few taps. The comparison is performed for different cladding panel sizes, considering a range of values for the filter scaling parameter $K$ for the TVL approach, and different selections of the pressure taps for the pneumatic averaging approach. An additional purpose of the research presented in this paper and in Lamberti et al. [17], is to make the high spatial resolution pressure data set for the determination of cladding loads on high-rise buildings available to the scientific community.

The remainder of this paper is organized as follows. Section 2 presents a summary of the experimental setup in the Politecnico di Milano wind tunnel, while Section 3 introduces the methodology for post-processing the wind tunnel data. The results are presented in Section 4, first providing an initial comparison of time histories of the pressure signal, before focusing on peak value analysis based on the TVL and the pneumatic averaging approaches. Section 5 presents the conclusions as well as suggestions for further research.

## 2. Experimental Setup

The experimental tests were carried out in the Boundary Layer test section of the close-circuit Politecnico di Milano wind tunnel. The facility has a cross-section equal to 14 m x 4 m and a length equal to 35 m (Figure 1). The building model has a rectangular base with dimensions 1 m x 0.3 m and it is 2 m high. It represents a generic high-rise building at a 1:50 length scale, corresponding to a 100 m tall building at full-scale. The choice of the 1:50 length scale supports obtaining a realistic representation of the reference full scale boundary layer profiles (mean velocity, turbulence intensities and integral length scales), while also enabling an accurate calculation of the area-averaged pressure on a typical cladding panel size given the pressure tap resolution on the model. The results presented in this paper have also been verified for a different length scale compatible with the ABL profiles adopted (e.g. using 1:100). The wind speed at building height was 11.7 m/s in the experiment; considering a full-scale design wind speed of 27.5 m/s, this implies a velocity scale equal to 1:2.35.

The measurements focused on the regions of the building where the highest peak pressures are expected: two aluminum tiles with 224 pressure taps each were placed in the top corner (tile A) and at the middle of the vertical edge of the model (tile B). The tap distance is 3 mm close to the building edges and increases progressively when moving away from the edges. The model was instrumented with 8 PSI ESP-32 HD high-speed pressure scanners, connected to a data acquisition system with a sampling frequency equal to 500 Hz. The outcome of each test is 300 s (model scale) pressure time histories — corresponding to more than 3500 convective times referring for normalization to the wind speed at building height and to the 1 m building width — , measured by the 446 pressure taps. The raw data for the pressure time-histories is post-processed by dividing the signal by the tubing frequency response function to account for the distortion introduced by the measurement system. The reference velocity is measured by a Pitot tube located 7 m upwind to the model. The pitot tube is located 1 m above ground; the measured velocity was corrected to be representative of the velocity at the building height. Table 1 summarizes the reference length and velocity as well as the sampling time and frequency at model- and full-scale. The analysis presented in this paper will focus on incoming wind directions in the range $-15°$ - $+30°$ and $-135°$ - $+150°$, with a 5° resolution, following the convention shown in Figure 1a.

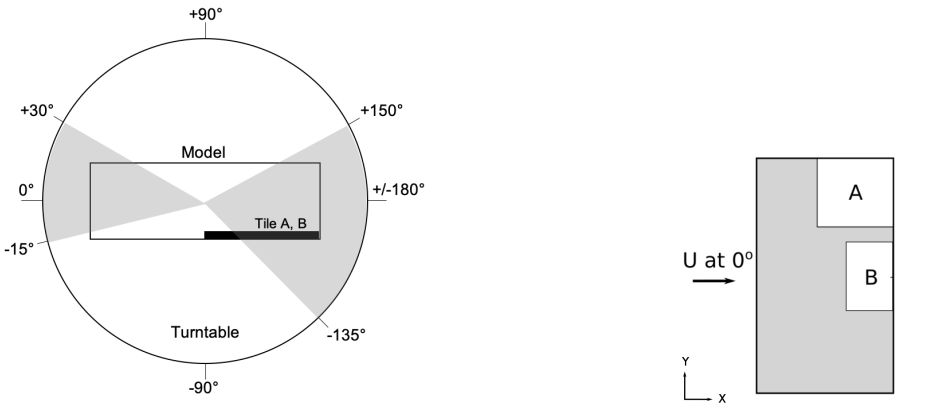


(a) Top view of the turntable, indicating the convention used for the wind direction. Grey areas show the wind directions tested

(b) Side view of the building model

Figure 1: Sketch of the building model.

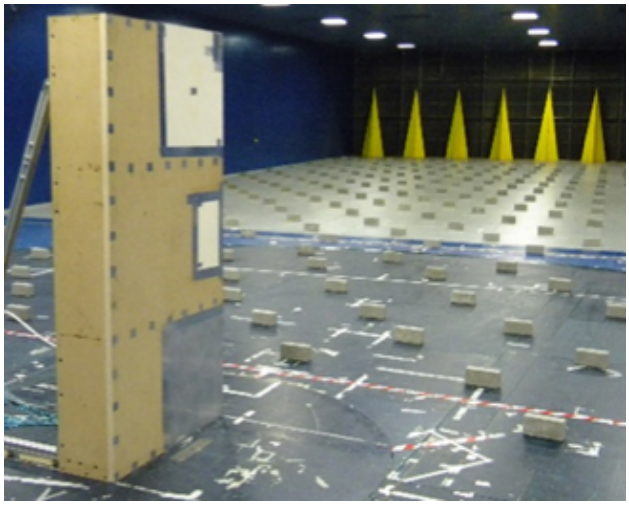

Figure 2: Building model in the Politecnico di Milano wind tunnel test section.

| | Model scale | Full scale |
|---|---|---|
| $H_{ref}$ | 2 m | 100 m |
| $U_{@H_{ref}}$ | 11.70 m/s | 27.5 m/s |
| Sampling time | 300 s | 6380 s |
| Sampling frequency | 500 Hz | 23.5 Hz |

Table 1: Reference height, reference velocity, sampling time and frequency for the wind tunnel tests.

### 2.1. Flow conditions

Correct scaling of the atmospheric boundary layer is essential to obtain representative wind pressure measurements on a structure. To generate a representative wind field, the experiments employed passive turbulence generators (a group of nine 2.5 m tall spires) at the inlet of the test section and roughness elements (bricks) on the wind tunnel floor upstream of the model, as shown in Figure 2. Velocity measurements were obtained across the test section at 5 different spanwise locations, spaced 0.6 m and symmetrically arranged with respect to the centre of the turntable. 20 s time histories of the three velocity components have been recorded using 3D hot-wires with a sampling frequency of 2000Hz.

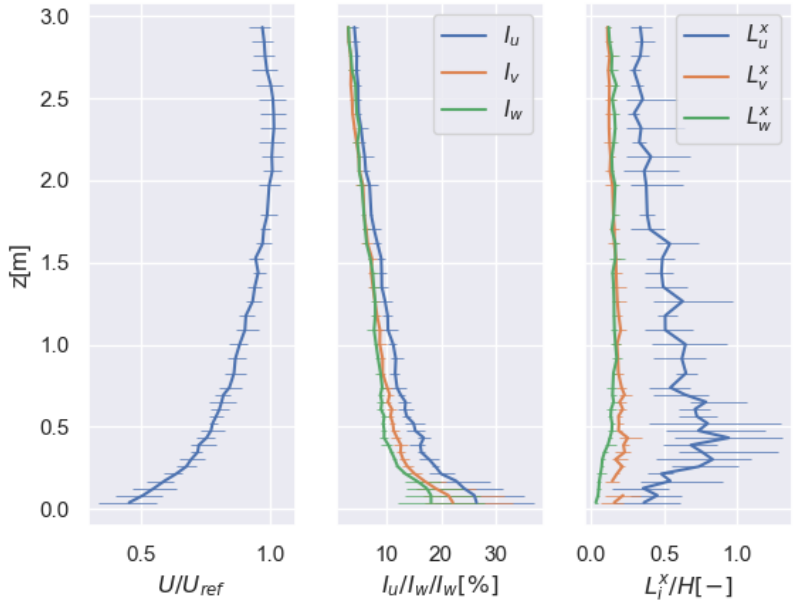


Figure 3: Wind profiles used for the wind tunnel tests. Left: mean speed profile. Centre: Turbulence intensity. Right: Integral length scales. Horizontal bars represents span-wise variation (min-max)

Figure 3 shows the resulting mean velocity (left), turbulence intensities (center), and length scales (right), averaged over the five span-wise locations. The error bars represent the span-wise variability of each quantity. The mean velocity profile U is normalized with respect to the reference velocity $U_{@H_{ref}}$. Comparison to a typical logarithmic mean velocity profile indicates that up to 2.4 m height good agreement is obtained for a roughness length of 1 mm model-scale, corresponding to a $z_0/H$ value of $5 \cdot 10^{-4}$. The integral length scales are computed using Taylor's hypothesis, taking the product between the mean stream-wise velocity and the integral time scale obtained from integration of the normalized auto-correlation function. The resulting length scale profiles differ from the typical ones proposed by the Eurocode or any other National Code, which normally increase with the height. This discrepancy indicates that the wind tunnel spectrum will not reflect the larger scales expected in a typical Eurocode spectrum, as is common in larger-scale model tests [18]. The absence of these larger scales is not expected to have an impact on the results presented in this paper; it was shown by Tieleman et al. [19] and further discussed by Farell et al. [20] that the mean and fluctuating pressures on the surfaces of rectangular prisms are primarily controlled by the small-scale turbulence content of the incident flow and, to a much lesser extent, by the integral scales of the turbulence, as long as the integral length scale is larger than the length scale of the area of interest (5m at

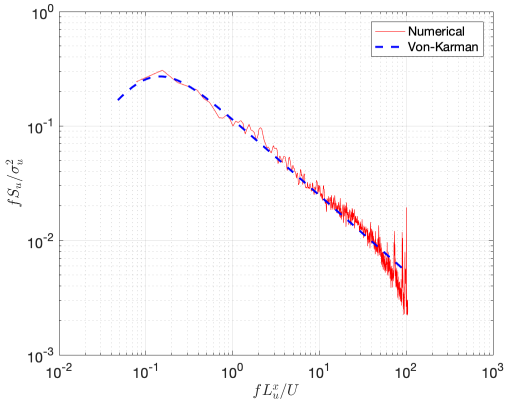


Figure 4: Streamwise velocity spectrum at 1 m height compared to the Von-Karman spectrum

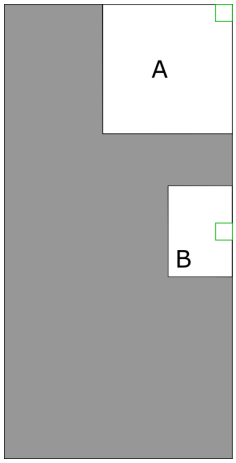


(a) Side view of the building model. The green areas include the 100 taps considered for the analysis.

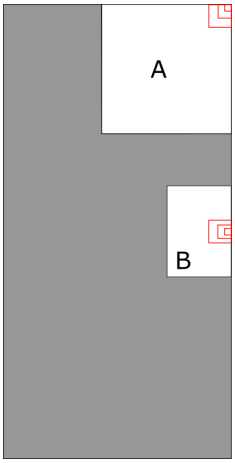


(b) Side view of the building model. The red squares represent the square panels considered for the analysis, i.e. with 1.5 m, 3 m and 5 m sides at full scale.

Figure 5: Schematic of the analysed regions on the building model.

full-scale in this study). The normalized streamwise velocity spectrum measured at 1 m height, shown in Figure 4, further indicates that a typical ABL turbulence spectrum is obtained; the spectrum compares well to the Von-Karman spectrum normalized by the measured integral length scale.

## 3. Methodology

The objective of this analysis is to assess the accuracy of the TVL approach for estimating the area-averaged pressure on cladding panels placed on the lateral facade of a high-rise building, at (1) the top corner, and (2) the edge at half the building height. Specifically, the analysis will focus on the regions indicated in Figure 5. We will consider the 100 taps closest to the top corner on Tile A, and the 100 taps closest to the edge at mid-height on Tile B. These regions are known to experience highly negative pressure peaks [17], and they have a sufficiently high spatial resolution of pressure taps to compute accurate area-averaged pressures on square panels of three different sizes (sides 1.5m, 3m, and 5m, full scale).

Table 2: Full-scale values of $\tau$ $[s]$ for different panel sizes and values of $K$

| | K = 0 | K = 1 | K = 2 | K = 3 | K = 4 | K = 4.5 | K = 5 |
|---|---|---|---|---|---|---|---|
| 1.5m x 1.5m | no filter | 0.08 | 0.15 | 0.23 | 0.31 | 0.35 | 0.39 |
| 3m x 3m | no filter | 0.15 | 0.31 | 0.46 | 0.62 | 0.69 | 0.77 |
| 5m x 5m | no filter | 0.26 | 0.51 | 0.77 | 1.03 | 1.16 | 1.29 |

### *3.1. Calculation of area-averaged and time-filtered pressure coefficients*

Throughout this paper, the pressure will be reported in non-dimensional form as a pressure coefficient:

$$C_p(t) = \frac{p(t) - p_{ref}}{\bar{q}_{ref}} \tag{2}$$

where $p_{ref}$ is the static reference pressure and $\bar{q}_{ref}$ is the average dynamic pressure measured at building height, computed as $\bar{q}_{ref} = \frac{1}{2}\rho(\bar{U}_{@Href})^2$ where $\rho$ is the air density. To support assessing the accuracy of the time-domain filtering technique and the pneumatic averaging technique, we will consider different time series derived from the raw pressure coefficient data:

1. The area-averaged pressure coefficient on a panel, $C_{p,AA}(t)$, calculated as:

$$C_{p,AA}(t) = \frac{\sum_{i=1}^{N} C_{p,i}(t) A_i}{A} \tag{3}$$

   where $C_{p,i}$ is the pressure coefficient recorded by the i-th tap, $A_i$ is its influence area and $A$ is the surface of the panel such that $A = \sum_{i=1}^{N} A_i$. Since the tributary area of each pressure tap is only few millimetres wide (model scale), the pressure is assumed to be constant on the tributary area.
2. The time-filtered pressure coefficient at a pressure tap, $C_{p,\tau}(t)$, calculated by applying a moving average filter to the raw data. The time span $\tau$ of the moving average filter is computed according to the TVL equation: $\tau = K \cdot L/V$, with $L$ equal to the diagonal of the panel, while $V$ is the reference velocity at the building height. The value of $K$ is varied from 0, corresponding to the unfiltered raw data, to 5; the corresponding full-scale values for $\tau$ are summarized in Table 2.
3. The pneumatic-averaged pressure coefficient at a pressure tap, $C_{p,pa}(t)$, calculated by averaging the signals obtained at 4 or 5 pressure taps on a panel, as depicted in configurations II and III in Figure 6. Configuration I, which uses the raw data obtained at the center of the panel, is included for reference.

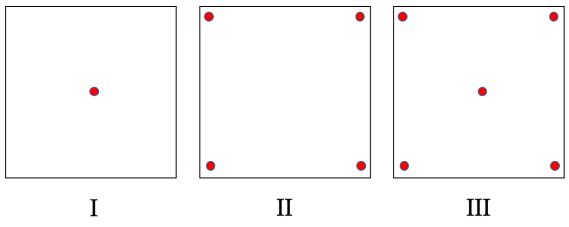


Figure 6: Configurations considered for the pneumatic-averaged pressure

### 3.2. Calculation of peak pressure coefficients

The presentation of the results will first consider a few snapshots of these different time series before focusing on the resulting estimates of the negative peak values $\check{C}_{p,AA}$, $\check{C}_{p,\tau}$, and $\check{C}_{p,pa}$. The difference between the peak values, $\check{C}_{p,AA} - \check{C}_{p,\tau}$, can then be computed to quantify the accuracy of the design pressure coefficient estimated from a single-point measurement using the TVL approach. Similarly, the accuracy of the pneumatic averaging approach can be determined from the difference $\check{C}_{p,AA} - \check{C}_{p,pa}$. The peak values are calculated following the extreme value analysis proposed by [21]. First, the 10 most negative uncorrelated events are extracted from each time-history, where two events are considered uncorrelated if they are at least 1 second apart in full-scale. Subsequently, these peaks are used to estimate the underlying extreme value parent distribution and compute the expected extreme value over 10 minutes full scale. We note that the resulting values have not been raised to any exponent; following the notation in [21] this corresponds to the use a power-law transformation $Z = X^w$ with $w = 1$. While this approach was originally developed for wind speed data, the underlying statistical methodology is valid for the estimation of the expected peak of any stationary process [22]. The method is also closely related to the Cook and Mayne approach [7].

## 4. Results

As discussed in Section 3, the presentation of the results focuses on comparing real area-averaged pressure coefficient data to the time-filtered TVL values and the pneumatically averaged values. The first subsection presents snapshots of the time series of $C_p$ to highlight the main qualitative differences between the time series. In the following two subsections, we focus on the quantitative differences in the peak pressure coefficients obtained from the TVL hypothesis and the pneumatic averaging, respectively. Since cladding design is often driven by the negative $C_p$ values (suction), the analysis will primarily focus on the wind directions that cause the extreme suction events, i.e. 10° for Tile A and 180° for Tile B [17]. Figure 7 shows the mean and negative peak pressure distribution on the two tiles for the considered wind directions; the mean negative $C_p$ values indicate that the tiles are in a region of flow separation, with the tile dimension much smaller than the separation region. For Tile A at 10°, the tile is located in the downwind top corner of the facade, while for tile B at 180°, the tile is located just downstream of the upwind corner at the building mid-height. For completeness, the analysis of the TVL hypothesis also includes a presentation of the differences in the envelope peak pressure coefficients that consider the minimum values across all wind directions.

### 4.1. Comparison of time histories

#### 4.1.1. Time histories on Tile A at 10°

Figure 8a presents 4 different snapshots of the time-histories recorded on tile A for the 10° wind direction. It considers a 1.5m by 1.5m panel, and compares the raw data acquired by a pressure tap placed near the top corner of the building to the one obtained using the TVL equation, to the area-averaged value, and to the pneumatically averaged pressure. The TVL approach used a full-scale time span $\tau$ equal to 0.34 s, obtained by assuming K equal to 4.5 and $L$ to the diagonal of the panel. The area-averaged value was computed by averaging the signals of the 49 pressure taps available on the panel. Finally, the pneumatic pressure was computed considering Configuration III (see Figure 6), by averaging 5 pressure taps on the panel. Figure 8b shows the same comparison for a 3m by 3m panel size. In this case, the TVL approach used $\tau$ equal to 0.69 s, again obtained using K equal to 4.5 and $L$ to the panel diagonal, and the area-averaged value was computed by averaging data from 91 taps. In both figures, the $x$ axis represents model-scale time.

The raw data exhibits several strong negative pressure peaks; the area-averaged time-history shows the same events but with a reduced peak magnitude of approximately 2-3 $C_p$. This indicates that a large event is

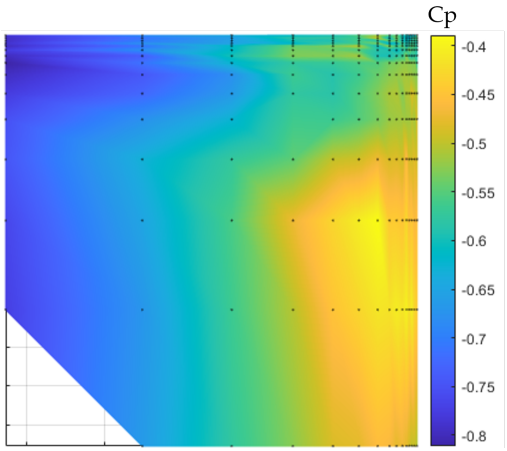


(a) Mean $C_p$ distribution in Tile A, wind direction +10°

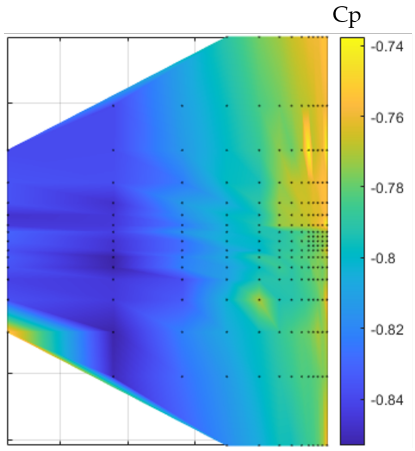


(b) Mean $C_p$ distribution in Tile B, wind direction 180°

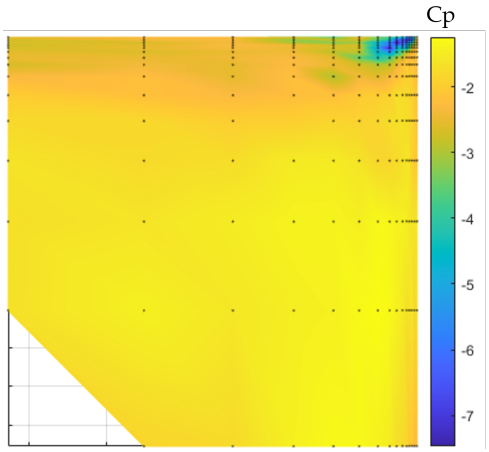


(c) Negative peak $C_p$ distribution in Tile A, wind direction +10°

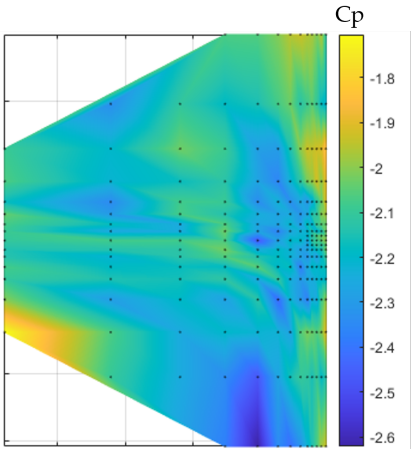


(d) Negative peak $C_p$ distribution in Tile B, wind direction 180°

Figure 7: Mean and peak $C_p$ pressure distribution for Tile A (a, c) and Tile B (b, d)

| | Event | raw data | TVL (K=4.5) | area-average | pneum. average |
|---|---|---|---|---|---|
| 1.5m x 1.5m | E1 | -4.43 | -2.72 | -2.36 | -2.02 |
| panel | E2 | -4.30 | -2.20 | -1.48 | -1.42 |
| | E3 | -4.23 | -3.05 | -2.02 | -1.73 |
| 3m x 3m | E1 | -4.43 | -2.00 | -1.83 | -2.12 |
| panel | E2 | -4.30 | -1.53 | -1.09 | -1.41 |
| | E3 | -4.23 | -3.06 | -1.83 | -1.74 |

Table 3: Comparison of negative pressure coefficients from raw data, from the TVL equation, and from area-average over a panel, and from pneumatic averaging for three suction events (see Figure 8).

affecting the entire panel area. During these large events, a shorter event affecting only an extremely small portion of the area with much higher amplitude is observed in the raw data. The latter are too small to affect the area-averaged load as shown by the blue lines in Figures 8a and 8b.

Focusing on Figure 8a, a clear difference between the blue line (area-averaged signal) and the pink line (TVL theory) is noticeable during the peak events. The signal processed using the TVL's moving average filter still presents more negative pressure peaks: in some cases, like events E1 and E2 in Figure 8, the peaks have been reduced by the TVL filter compared to the raw signal. However, there are instances, like event E3, where the moving average does not impact the magnitude of the peak. The area-averaged signal does exhibit a reduced peak magnitude, indicating that these events, although longer-lived, are spatially small and do not affect the area-average pressure significantly. Such finding indicates that for these events the ratio between the spatial size and the time duration is much different from the one predicted by the TVL equation: while their duration is larger than the value of $\tau$, their size is much smaller than the panel size.

The pneumatically averaged signal compares well to the area-averaged pressure in the time intervals of Figure 8. Focusing on peak events E1 and E2, the pneumatic average is able to reflect the area-averaged signal, with a slight overestimation for the 3m side panel. In case of slower event E3, a small discrepancy is found for the 1.5m panel.

Table 3 reports the peak values for the two strongest short-lived suction events in the second snapshot (indicated by E1 and E2 in Figure 8), and for the longer duration event in the fourth snapshot (E3 in Figure 8). For the short-lived events on the 1.5m panel, the TVL equation reduces the locally measured peak value by 38% and 49%, while area-averaging results in a reduction of 47% and 66%, respectively. When compared to the pneumatic average values, such reductions increase to 54% and 67%. For the longer duration event, the TVL formula results in a negligible reduction of the peak value over most of the duration of the event, while the area-averaged and the pneumatic averaged values are 50% and 60% lower than the raw data. For the larger 3m panel, the same observation holds: the area-average peak value is significantly lower than the values obtained from the TVL equation.

Overall, the time series presented in this section indicate that the raw data obtained at a single pressure tap has high-frequency content that is not representative of the pressure acting over the surface area of a cladding panel. The TVL equation with the standard value of K equal to 4.5 fails to make the single tap signal an accurate representation of the area-averaged one; pneumatic averaging over a few taps seems to provide a more representative result.

#### *4.1.2. Time histories on Tile B at 180°*

Considering Tile B for the 180° wind direction, Figure 9 presents a comparison of the raw data acquired by a pressure tap placed at mid-height near the edge of the building to the values obtained using the TVL

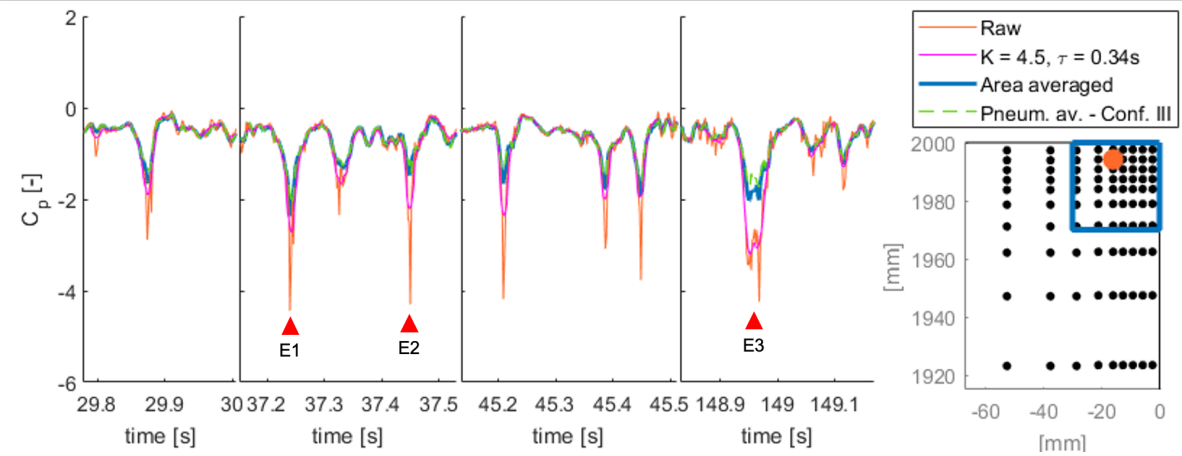


(a) Time histories comparison when the area averaged pressure is computed for a 1.5m by 1.5m panel

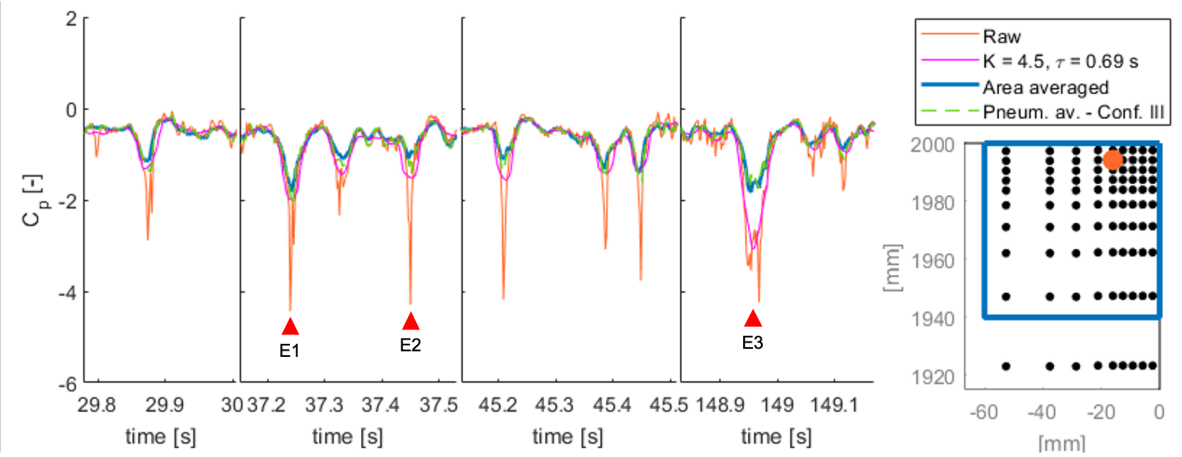


(b) Time histories comparison when the area averaged pressure is computed for a 3m by 3m panel

Figure 8: Comparison between the raw signal of one pressure tap on tile A, the same but filtered by the moving average operator, the area-averaged value, and the pneumatic averaged value on a 1.5m by 1.5m panel (a) and on a 3m by 3m panel (b), wind direction 10°. The maps on the right show the selected pressure tap.

equation, to the area-averaged values, and to the pneumatic averaged pressure. The latter is computed considering 5 taps (Configuration III), as shown in Figure 6. For most of the time, the pressure time series is largely unaffected by the area-averaging, and the TVL equation produces an accurate representation of the area-averaged value. Only one event, at $t$ = 116 s, is significantly affected by the area-averaging; during this event the TVL equation remains relatively accurate with $\sim$10% difference in the prediction of the peak value. The pneumatic averaged pressure reflects the area-averaged value for any peak event.

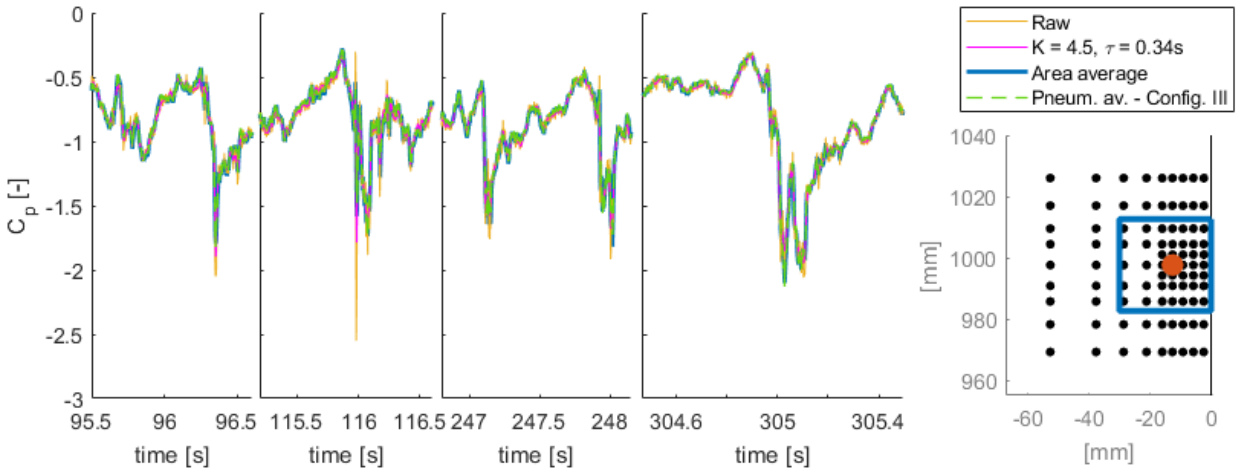


(a) Time histories comparison when the area averaged pressure is computed for a 1.5m by 1.5m panel

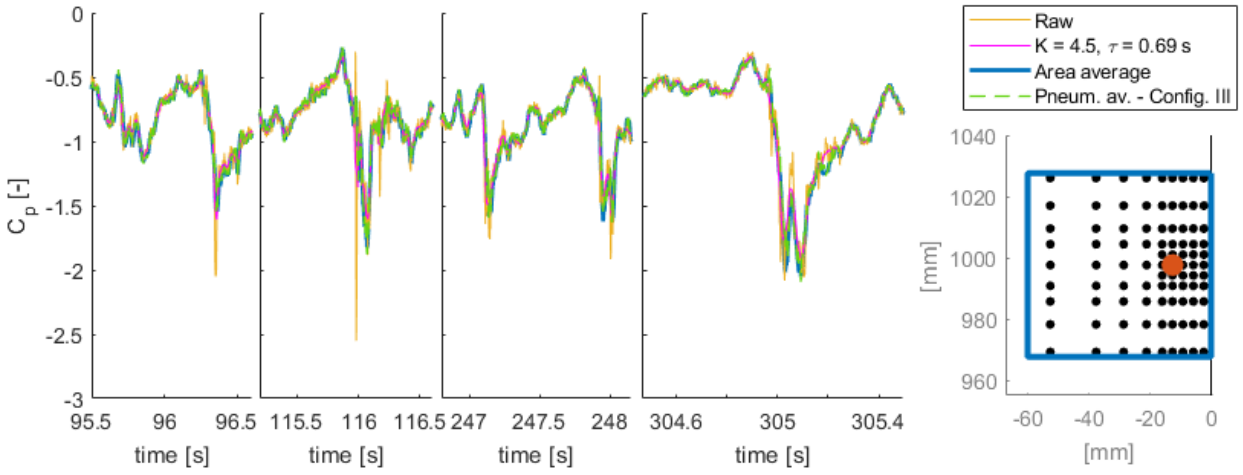


(b) Time histories comparison when the area averaged pressure is computed for a 3m by 3m panel

Figure 9: Comparison between the raw signal of one pressure tap on tile B, the same but filtered by the moving average operator, the area-averaged value, and the pneumatic averaged value on a 1.5m by 1.5m panel (a) and on a 3m by 3m panel (b), wind direction 180°. The maps on the right show the selected pressure tap.

This result is strikingly different from the observations on Tile A for the 10° wind direction. The raw data is significantly more representative of the pressure acting on a cladding panel, indicating that the pressure signal in the separation region just downstream of the windward edge has a stronger spatial correlation. The TVL equation with K=4.5 seems to provide an appropriate representation of the area-averaged value, with the difference between the area-averaged peak events and the ones predicted by the

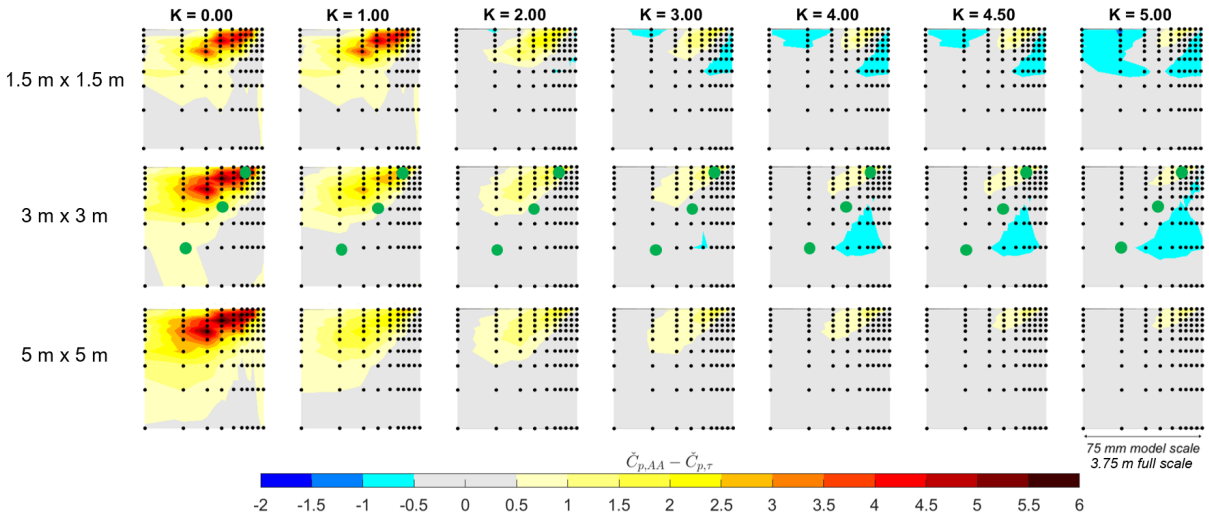


Figure 10: Contour plots of the difference between the values of $\check{C}_{p,AA}$ and $\check{C}_{p,\tau}$ for 10° on Tile A. Green dots show the position of the taps listed in Table 4.

filtered signal always less than 10%.

### *4.2. Analysis of time-filtered peak values obtained using the TVL approach*

In this section, we analyze the difference between the peak values estimated from the area-averaged signal ($\check{C}_{p,AA}$) and the time-filtered signal ($\check{C}_{p,\tau}$). For the area-averaging, we now consider three panel sizes, i.e. square panels with a side of 1.5 m, 3 m and 5 m. For the time-filtering, we consider values of K ranging from 1 to 5. The corresponding values of $\tau$ for each panel size are computed according to Eq. 1 and reported in Table 2. This analysis will support identifying if there is a value for $K$ that minimizes the difference $\check{C}_{p,AA} - \check{C}_{p,\tau}$.

#### *4.2.1. Comparison of area-averaged and time-filtered peak values on Tile A - 10° wind direction*

Figure 10 shows the spatial distribution of the difference $\check{C}_{p,AA} - \check{C}_{p,\tau}$ in the analyzed region of Tile A for the 10° wind direction. The different rows present the results for the three different panel sizes considered, while the columns depict different values of $K$. In this plot, a positive value for $\check{C}_{p,AA} - \check{C}_{p,\tau}$ means that the peak value computed by applying the TVL theory overestimates the magnitude of the real, area-averaged, peak value (i.e. $\check{C}_{p,\tau}$ is more negative than $\check{C}_{p,AA}$). Vice versa, a negative difference means that the peak value computed from the TVL theory is underestimating the magnitude of the area-averaged peak value (i.e. $\check{C}_{p,\tau}$ is less negative than $\check{C}_{p,AA}$).

Figure 10 indicates that using the raw pressure signal ($K = 0$) recorded at taps in the top corner region leads to severe overestimations of the area-averaged peak pressure magnitudes on a panel: the design value obtained from the raw data can be more than 5 $C_p$ more negative than the area-averaged value for all panel sizes. The area where these high errors occurs increases with the panel size, since the spatial averaging operation results in lower peak magnitudes as the averaging area increases. Moving away from the building corner, the 1.5 $m$ and 3 $m$ cases have some pressure taps that are characterized by small differences, with $\check{C}_{p,AA} - \check{C}_{p,\tau}$ in the $\pm 0.5\ C_p$ range. For the 5 $m$ panel, the differences remains slightly higher over most of the tile, in the range of $\approx 2\ C_p$. Considering the results for $K = 1$, the difference $\check{C}_{p,AA} - \check{C}_{p,\tau}$ decreases, except for the smallest panel. In this case the time-filtering has a negligible effect since the model scale value of

| tap location | $K = 0.0$ | $K = 1.0$ | $K = 2.0$ | $K = 3.0$ | $K = 4.0$ | $K = 4.5$ | $K = 5.0$ |
|---|---|---|---|---|---|---|---|
| close to top corner | 4.87 | 2.82 | 1.67 | 1.41 | 1.24 | 1.24 | 1.12 |
| 3m panel center | 1.01 | 0.62 | 0.26 | 0.077 | -0.083 | -0.083 | -0.17 |
| 3m panel edge | 0.61 | 0.31 | -0.038 | -0.23 | -0.38 | -0.38 | -0.43 |

Table 4: The difference $\check{C}_{p,AA} - \check{C}_{p,\tau}$ for a tap close to the top corner, for a tap at the 3m panel center and for a tap further away from the building edges (see Figure 10 for tap locations).

$\tau$ corresponds to only twice the sampling time. As the $K$ value - and, accordingly, $\tau$ - further increases, the overestimation of the area-averaged peak pressure further decreases. For the value proposed by Lawson ($K = 4.5$), the TVL estimated extreme values are less than 1 $C_p$ different from the area-averaged values in most pressure taps. Only in a small region close to the top corner, where the strongest negative peak events occur, an overestimation of $\sim 1.5\ C_p$ is still observed. For the 1.5m and 3m panels, a small (less than $1C_p$) underestimation of the area averaged peak pressure at a few locations.

Table 4 reports the difference $\check{C}_{p,AA} - \check{C}_{p,\tau}$ for three tap locations the 3m panel, indicated by the green dots in Figure 10: a tap close to the building edge, one at the center of the panel and another one placed in the lower left corner of the same panel. The values confirm that taps close to the top corner of the building lead to a severe overestimation of the area-averaged peak pressure for all values of $K$. Conversely, taps further away from the corner and edges can predict a representative design $C_p$ when the TVL formula is applied, although the optimal value of $K$ is dependent on the tap location.

To further visualize how the difference between $\check{C}_{p,AA}$ and $\check{C}_{p,\tau}$ changes with $K$ in different locations, a violin plot [23, 24] is included in Figure 11. The figure only depicts the results obtained for the 3m panel, since the observed trends are representative for all three panel sizes considered in this study. For each value of $K$, a box plot is shown together with a kernel density plot, estimated for the error population. Each subplot also includes the actual distribution of the error values, where the color of the points indicates the spatial location of the pressure tap following the color code shown in the tile depicted on the right-hand side. The plot identifies three groups of pressure taps, split along the panel diagonal, that behave differently as a function of $K$. The blue colored pressure taps in the upper triangle exhibit both the strongest spatial dependency and the strongest dependency on the time-filtering. As the value of $\tau$ increases, the spatial dependency decreases and the maximum differences $\check{C}_{p,AA} - \check{C}_{p,\tau}$ decrease from more than 5 $C_p$ to less than 2 $C_p$. For all taps in this group and for all values of $K$ considered, the use of the TVL assumption would result in an overestimate of the peak design load. Moving down to the red taps in the lower triangle along the vertical edge of the building, the results exhibit less spatial dependency as well as a less strong effect of the time-filtering, The differences $\check{C}_{p,AA} - \check{C}_{p,\tau}$ remain in the range $\pm 0.5 C_p$ across all taps in this group for values of $K \geq 1$. The pressure taps in this area define the lower tail of the distribution, resulting in an underestimate of the peak design load for $K > 1$. Lastly, the green pressure taps along the diagonal and farthest from the corner show a behaviour similar to the red taps, but with slightly higher values of $\check{C}_{p,\tau}$. In these locations, the TVL equation provides a good estimate for the peak design pressure using $K \approx 3$.

The distinctly different effect of an increase of $\tau$ in the upper and lower triangles on the panel suggests a difference in the physical nature of the peak events in these regions. Across the upper triangle, the significant decrease in the variability of the values when $\tau$ increases is indicative of short-lived peak events that are strongly reduced by the time-filtering. Across the lower triangle, the reduced influence of $\tau$ indicates that the signals are characterized by peak events with a longer duration, for which the time-filtering is less effective. Some pressure taps in the upper triangle consistently exhibit a large value of around 2 $C_p$ for $\check{C}_{p,AA} - \check{C}_{p,\tau}$, independently from the value of $K$ considered. It was verified that the dynamic part of the

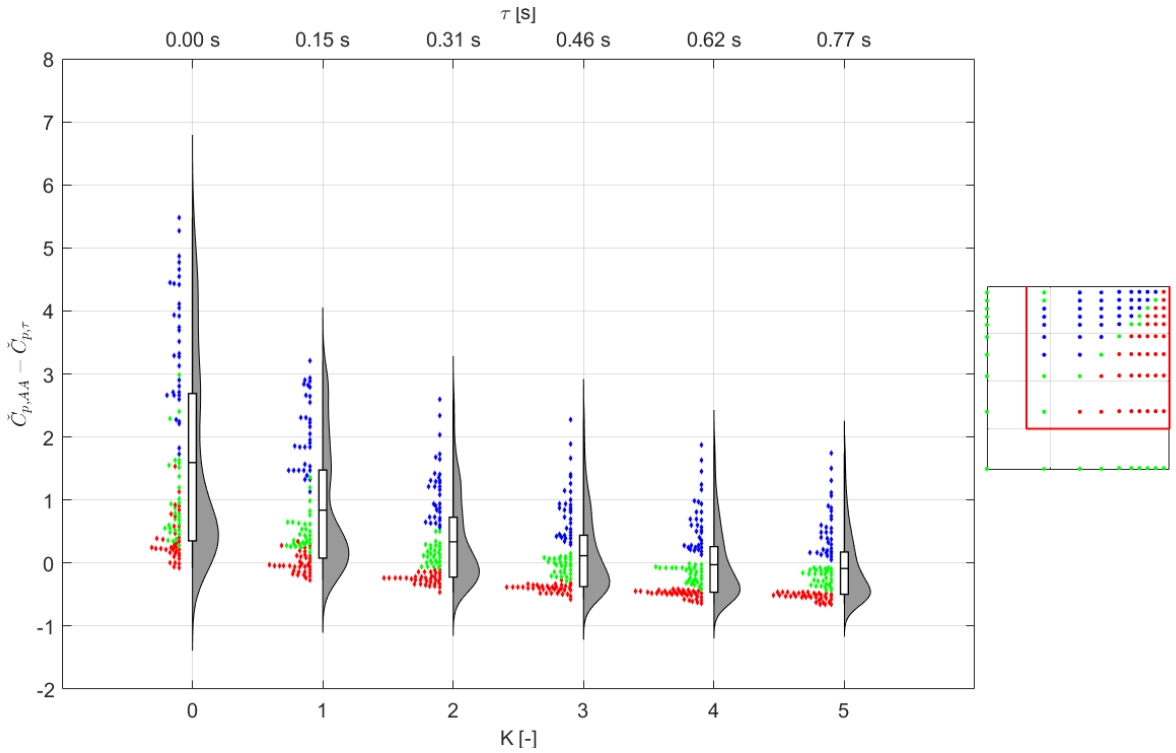


Figure 11: Violin plot of the difference between the values of $\check{C}_{p,AA}$ and $\check{C}_{p,\tau}$ for 10° when a panel size 3m x 3m is considered on Tile A region.

signal is the main source of the difference in the peak values by verifying good agreement (within $\pm 0.2\, C_p$) between the mean values of the pressure time series recorded by a single pressure tap and the mean value of the area-averaged signal. Consequently, the time-averaging procedure using the TVL equation might not be applicable in the region near the top edge.

### *4.2.2. Tile A - envelope diagrams*

In the previous sections, the analysis focused on a single wind direction. Since design values are generally computed as the most negative pressure occurring among all wind directions, this section presents the envelope diagram. This diagram consider the difference between the lowest value of the area-averaged and time-averaged peak pressure coefficients among all the wind directions:

$$Err = \min_{\theta} \check{C}_{p,AA}(\theta) - \min_{\theta} \check{C}_{p,\tau}(\theta) \tag{4}$$

Using this definition, the minimum area-averaged values across all wind directions are used as the reference values. It is worth noting that Eq. 4 considers that the most negative values for $\check{C}_{p,AA}$ and $\check{C}_{p,\tau}$ may occur for different wind directions; this is intentional, since the objective is to analyse the error in the final design value that is obtained when using time-filtered single pressure tap data versus when using the actual area-averaged pressure on a panel.

Figure 12 shows the contour plots of the difference between the minimum values of $\check{C}_{p,AA}$ and $\check{C}_{p,\tau}$ across all wind directions. The different rows present the results for the three different panel sizes considered, while the columns depict different values of $K$, and correspondingly $\tau$ (see Table 2). For $K = 0.0$, i.e. the raw data, the envelope peak pressure coefficients calculated from the taps experiencing the strongest peak

events exhibit the highest difference from the area-averaged values. For the largest panel size considered, the overestimation reaches a magnitude of 6 $C_p$. When increasing the $K$ value, the pressure taps in the top corner region continue to show positive differences, indicating that the TVL theory still results in an overestimation of the real area-averaged peak pressure magnitude. This finding holds across all panel sizes. For pressure taps further away from the corner, an increase in the $K$ value does reduce the difference with the area-averaged values: in all gray-colored regions, the difference is in the range $-0.5$ - 0.5 $C_p$. For the 1.5 $m$ and 3 $m$ panels, however, several pressure taps exhibit negative values of the difference between the minimum values of $\check{C}_{p,AA}$ and $\check{C}_{p,\tau}$, in the range $-0.5$ to $-1.5$ $C_p$, indicating that in these locations the TVL theory results in an underestimation of the envelope design pressure coefficients.

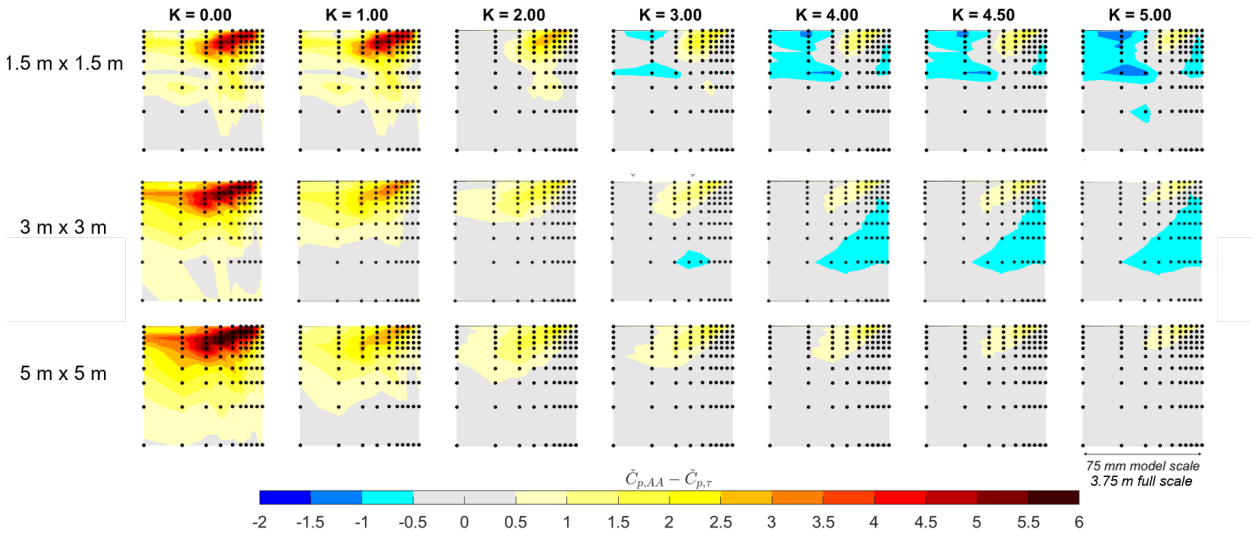


Figure 12: Contour plots of the difference between the minimum values of $\check{C}_{p,AA}$ and $\check{C}_{p,\tau}$ for all wind directions on Tile A.

The results in Figure 12 are consistent with those in Figure 10. They indicate that the "optimum" value of $K$, i.e. the one that minimizes the difference between the peak value estimated from the time-filtered signal ($\check{C}_{p,\tau}$) and the peak value estimated from the real area-averaged signal ($\check{C}_{p,AA}$), depends on the position of the pressure sensor and on the size of the panel. Figure 13 visualizes this dependency through a contour plot of the value of $K$ that minimizes this difference at each pressure tap. The optimal $K$ value for the pressure taps near the top edge is up to 5 times higher with respect to other locations. When avoiding these areas, the optimal $K$ values fall in the range 1 - 4.

*4.2.3. Comparison of area-averaged and time-filtered peak values on Tile B - Wind direction 180 degrees*

Figure 14 shows the spatial distribution of the difference $\check{C}_{p,AA} - \check{C}_{p,\tau}$ in the analyzed region of Tile B for the 180° wind direction. The different rows again present the results for the three different panel sizes considered, while the columns depict different values of $K$. Compared to Tile A at 10°, it is worth noting that the differences between $\check{C}_{p,AA}$ and $\check{C}_{p,\tau}$ assume much smaller values. This could be expected since the pressure signals on tile B do not exhibit the very strong, but short-lived and localized, peak events observed on Tile A (see section 4.1 and [17]).

For $K$ equal to 0, i.e. when $\check{C}_{p,\tau}$ is equal to the raw signal, the difference with $\check{C}_{p,AA}$ indicates a consistent overestimate of the area-averaged peak pressure magnitude, but the difference never exceeds $1C_p$. When

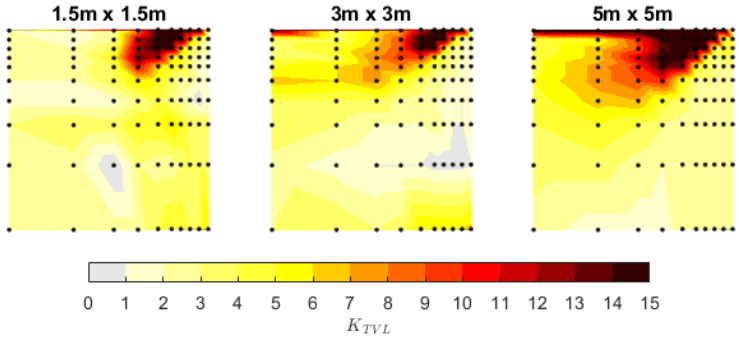


Figure 13: Contour plots of the value for $K$ that minimizes the difference between the minimum values of $\check{C}_{p,AA}$ and $\check{C}_{p,\tau}$ for all wind directions on Tile A.

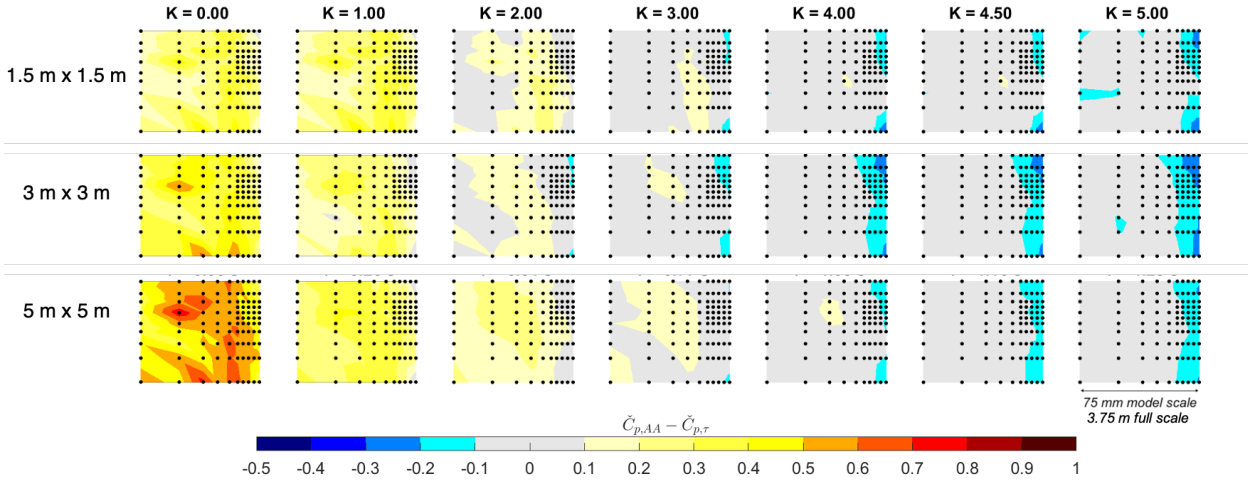


Figure 14: Contour plots of the difference between the values of $\check{C}_{p,AA}$ and $\check{C}_{p,\tau}$ for 180° on Tile B.

increasing the $K$ value, the difference starts to assume both positive and negative errors in the range $\pm 0.3 C_p$. For values of $K$ higher than 4, the time series recorded at the taps closest to the building edge lead to an underestimation of the area-averaged peak values for all the panel sizes considered; the data recorded at all other taps matches the value of $\check{C}_{p,AA}$ within $\pm 0.1\ C_p$.

Figure 15 presents the violin plot for the 3m panel to further visualize how the difference between $\check{C}_{p,AA}$ and $\check{C}_{p,\tau}$ changes with $K$ in different locations. For the other panel size, similar behavior was observed. The plot confirms that for $K$ equal to 0 or 1, $\check{C}_{p,\tau}$ consistently overestimates the area-averaged peak pressure magnitude, but the difference never exceeds $0.7 C_p$. When increasing the $K$ value, the value of $\check{C}_{p,\tau}$ decreases, resulting in small differences with $\check{C}_{p,AA}$ in the range $\pm 0.25 C_p$. For these higher values of $K$ two different regions seem to appear: the pressure taps closer to the edge (red dots) form the lower tail, representing an underestimation of $\check{C}_{p,AA}$ while those further away from the edge (green dots) form the upper tail, representing an overestimation of $\check{C}_{p,AA}$. Comparison of the mean values of the pressure time series recorded by a single pressure tap to the mean value of the area-averaged signal revealed an agreement within

$\pm 0.06\ C_p$, excluding that differences in the mean values are responsible for such errors. Hence, these two regions seems to indicate a shift in the dynamic behavior immediately downwind of the windward corner vs slightly further downstream, but the differences are far less pronounced than on Tile A.

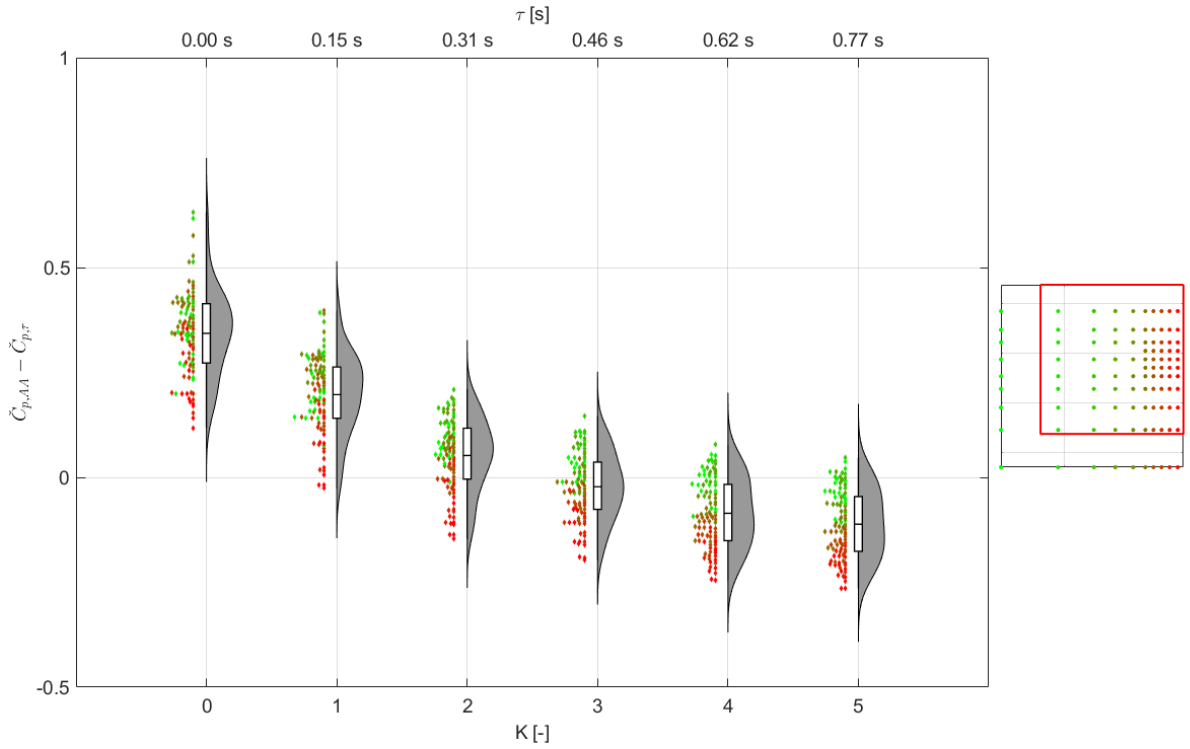


Figure 15: Violin plot of the difference between the values of $\check{C}_{p,AA}$ and $\check{C}_{p,\tau}$ for 180° when a panel size 3m x 3m is considered on Tile B region.

### *4.2.4. Tile B - Envelope Diagram*

Figure 16 shows the contour plots of the difference between the minimum values of $\check{C}_{p,AA}$ and $\check{C}_{p,\tau}$ across all wind directions on Tile B. The different rows present the results for the three different panel sizes considered, while the columns depict different values of $K$, and correspondingly $\tau$ (see Table 2). The plots confirm the findings of the analysis for the 180° wind direction in section 4.2.3: the differences are much smaller ($< 1.2\ C_p$) than on tile A, and they vary from a consistent overestimation of the area-averaged peak value for $K = 0$ (i.e. using the raw pressure tap data) to a slight underestimation for higher values of $K$, in particular for the taps closest to the building edge.

Figure 17 presents the contour plot showing the optimal value of $K$ for each pressure tap on the tile B, for each panel size. In this case, the range of $K$ is limited to 4 - 6, indicating that the original formulation by Lawson ($K = 4.5$) is adequate for this region at the building mid-height.

## *4.3. Analysis of pneumatically averaged peak values obtained using a few pressure taps*

In this section, we analyze the difference between the peak values estimated from the area-averaged signal ($\check{C}_{p,AA}$) and the pneumatic averaged signal ($\check{C}_{p,pa}$). As in the previous section, we consider three panel sizes, i.e. square panels with a side of 1.5 m, 3 m and 5 m. For the pneumatic averaging we consider configurations including 4 and 5 pressure taps, as shown in Figure 6. The case with one single pressure tap at the center of the panel is also included for reference.

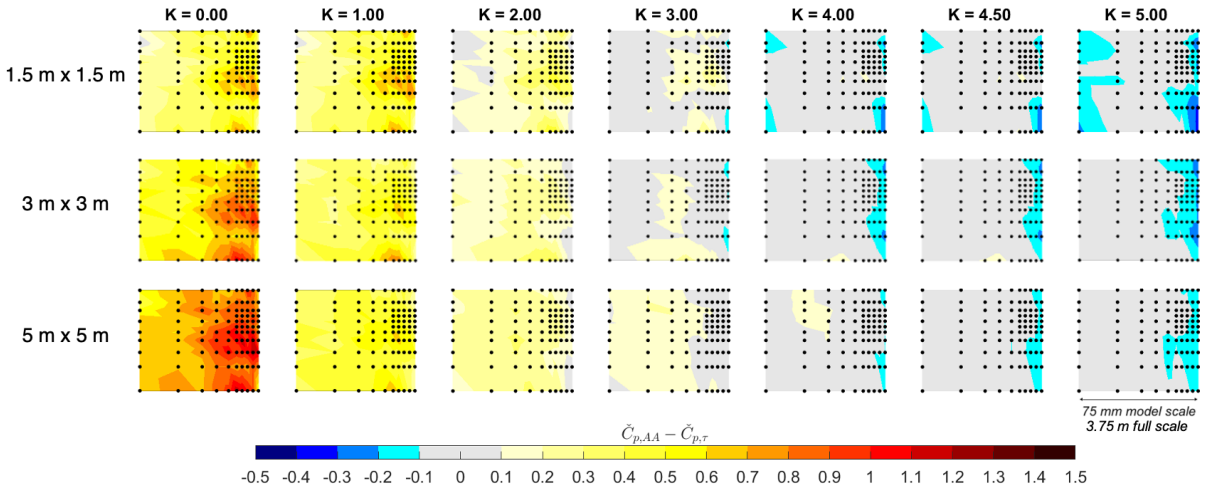


Figure 16: Contour plots of the difference between the minimum values of $\check{C}_{p,AA}$ and $\check{C}_{p,\tau}$ for all wind directions on Tile B.

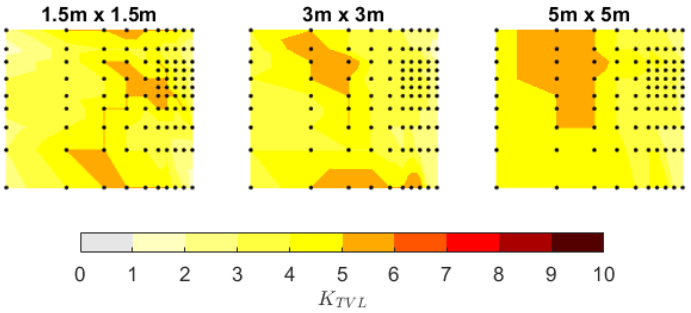


Figure 17: Contour plots of the value for $K$ that minimizes the difference between the minimum values of $\check{C}_{p,AA}$ and $\check{C}_{p,\tau}$ for all wind directions on Tile B.

*4.3.1. Comparison of area-averaged and pneumatically averaged peak values on Tile A - 10° wind direction*

Table 5 presents the comparison of the peak pressure coefficients for the top corner of Tile A, considering the 10° wind direction. Configurations II and III are shown to offer significant improvements in the estimate of $\check{C}_{p,AA}$ compared to the use of only one pressure tap at the center (Configuration I). The latter results in an overly conservative estimate of the peak pressure coefficient, with discrepancies between $1C_p$ and $2.5C_p$ for the different panel sizes. In contrast, pneumatic averaging using Configurations II and III correctly reflects the reduction in the area-averaged peak value as the panel size increases. The difference between Configurations II and III in terms of peak pressure coefficients is small, indicating that for this panel location, 4 pressure taps located in the corners of the panel can adequately represent the average pressure.

Table 5: Comparison of negative peak pressure coefficients of area-average and pneumatic average values for considered configurations on tile A region. Wind direction is 10°.

| panel size | $\check{C}_{p,AA}$ | $\check{C}_{p,pa\ I}$ | $\check{C}_{p,pa\ II}$ | $\check{C}_{p,pa\ III}$ |
|---|---|---|---|---|
| 1.5m x 1.5m | -2.43 | -4.97 | -2.16 | -2.14 |
| 3m x 3m | -1.97 | -2.99 | -1.72 | -1.74 |
| 5m x 5m | -1.56 | -2.58 | -1.43 | -1.45 |

#### *4.3.2. Comparison of area-averaged and pneumatically averaged peak values on Tile B - 180° wind direction*

Table 6 shows the comparison between the area-averaged peak pressure and the pneumatic averaged values for panels near the edge of Tile B, considering the 180° wind direction. For this location and wind direction, the discrepancies when using a single pressure tap at the center range from $0.5C_p$ to $0.25C_p$. When using the pneumatic averaged pressure obtained with Configurations II and III, the maximum observed difference is reduced significantly to $0.03C_p$. As on Tile A, the difference between Configuration II and III is negligible, indicating the 4 pressure taps near the corners can provide a good approximation of the area-averaged pressure on a tile in this location. The results presented in this section indicate the promising potential of pneumatic averaging as an alternative to the use of the TVL theory for cladding design wind tunnel tests.

Table 6: Comparison of negative peak pressure coefficients of area-average and pneumatic average values for considered configurations on tile B region. Wind direction is 180°.

| panel size | $\check{C}_{p,AA}$ | $\check{C}_{p,pa\ I}$ | $\check{C}_{p,pa\ II}$ | $\check{C}_{p,pa\ III}$ |
|---|---|---|---|---|
| 1.5m x 1.5m | -1.80 | -2.05 | -1.78 | -1.79 |
| 3m x 3m | -1.75 | -2.07 | -1.76 | -1.75 |
| 5m x 5m | -1.68 | -2.18 | -1.71 | -1.70 |

## 5. Conclusions

This paper has presented an analysis of high-resolution pressure tap measurements for peak cladding load estimation on a high-rise building. The analysis focused on panels near the top corners and edges of the building's lateral façade, where suction peaks are the determining factor for cladding design. The high-resolution measurements were used to calculate the real area-averaged pressure on the panels. This value was then compared to the values obtained using a moving-average filter with a time-scale based on the commonly adopted TVL equation and to the values obtained using pneumatic averaging over a few pressure taps on a tile. The comparison was performed for three different cladding panel sizes. The evaluation of the TVL equation considered a range of values for the filter time-scale $\tau = K \cdot L/V$ by varying $K$ between 0 and 5. Previously proposed versions of the moving average filter have applied $K = 4.5$ (the Lawson formulation) or $K = 1$ (the Holmes formulation). The evaluation of the pneumatic averaging considered two different tap configuration, either including 4 taps near the panel corners, or adding an additional tap at the panel center.

Considering the panel near the vertical edge at mid-height, the magnitude of the suction peaks is on the order of -2 $C_p$, and the results support the validity of the TVL equation. In this location, the standard use of the Lawson formulation results in errors less than $\pm 0.25$ $C_p$ for all pressure taps considered. The

errors primarily result in an underestimate of the peak design load, which is largest when using pressure taps closest to the building edge. In contrast, use of the Holmes formulation results in an overestimate of the peak design load at nearly all pressure taps. The maximum difference of 0.4 $C_p$ occurs when using the taps closest to the edge. Use of pneumatic averaging can improve the accuracy of the peak estimates, with errors below 0.03 $C_p$.

Considering the panel near the top corner, stronger suction events with peaks on the order of -5 $C_p$ are observed, and the results reveal much larger errors when using the TVL equation. The high resolution of the pressure taps allowed to investigate the extremely strong pressure peak events that affect the downstream top corner region on the lateral facade at 10° wind direction. These events were shown to be localized in the area above the corner's bisector line. They are characterized by a spatial size significantly smaller than the panel size, but their duration is longer than what would be expected based on the TVL equation. As a result, the moving average filter does not correctly reduce the magnitude of these peaks in the signal. The standard use of the Lawson formulation would lead to errors in the peak pressure coefficient of $\pm 1$ $C_p$ in most locations, except for a few pressure taps closest to the top edge and corner where overestimates of up to 2 $C_p$ can occur. Use of the formulation by Holmes would mostly result in conservative design values, with overestimates up to 4 $C_p$ for pressure taps above the corner's bisector line, and underestimates of less than 0.2 $C_p$ for pressure taps below that line. As a potential alternative to use of the TVL equation, pneumatic averaging was found to improve the accuracy of the peak estimates, with errors below 0.3 $C_p$.

The severe errors that can occur when applying the TVL approach to pressure taps in the top corner region are concerning, because in practice the results between the tap closest to the edge and the adjacent tap that can be several metres (full scale) away are often interpolated. In this case, overestimation of the design pressure by a single tap can cause a large portion of the cladding surface to be overdesigned. In the authors' experience, this type of behaviour and these events have been observed in several commercial wind tunnel tests in proximity of façade vertices, leading to an over-conservative design that negatively impacts the total building costs. A simple workaround could be to avoid to position pressure taps close to the building edges, where the design values obtained using the TVL equation present the largest errors. However, further analysis of the minimum distance at which taps need to be placed under different flow conditions has to be performed. In addition, the results do suggest that the region closest to the building edge is affected by extremely strong suction events with a very limited spatial extension. Hence, any structural/façade element that would be placed in such region should be carefully designed to withstand the corresponding loads.

Finally, it is worth considering the implications of the fact that the optimum value of $K$, i.e. the one that leads to the smallest difference between the estimated peak value and the real area-averaged value, depends both on the location of the pressure tap and on the panel size considered. From a conceptual point of view, this indicates that a moving average time-filter with a time-scale linearly proportional to $L/V$ cannot correctly represent a universal aerodynamic admittance function. At the very least, as also pointed out by Holmes [6], the proportionality coefficient cannot be assumed to be independent of the panel size or the region on the façade considered. In addition to the variability across the building facade, the wind characteristics could further affect the optimal K values reported in this study. The pneumatic averaging approach provided accurate results for all panel sizes and for both locations in this study, which indicates that it could potentially provide a more robust approach to estimating cladding loads near corners and edges. Further research should therefore focus on evaluating the accuracy of the estimates obtained with the TVL hypothesis and with pneumatic averaging considering different high-rise building shapes, different locations on the facades, and different turbulence characteristics.

# References


[1] M. Overend, K. Zammit, Wind loading on cladding and glazed façades, in: International Symposium on the Application of Architectural Glass, ISAAG, 2006, pp. 1–10.

[2] F. Rigo, T. Andrianne, V. Denoël, Mixture model in high-order statistics for peak factor estimation on low-rise building, in: Conference of the Italian Association for Wind Engineering, Springer, 2018, pp. 613–629.

[3] T. Lawson, The design of cladding, Building and Environment 11 (1976) 37–38.

[4] T. V. Lawson, Wind Effects on Buildings: Design Applications, volume 1, Spon Press, 1980.

[5] C. W. Newberry, K. J. Eaton, J. Mayne, Wind loading on tall buildings: further results from Royex House, Building Research Establishment, Building Research Station, 1973.

[6] J. D. Holmes, Equivalent time averaging in wind engineering, Journal of Wind Engineering and Industrial Aerodynamics 72 (1997) 411–419.

[7] N. J. Cook, The designer's guide to wind loading of building structures. vol. 2: Static structures, Building Research Establishment Report, London: Butterworth,— c1990 (1990).

[8] J. D. Holmes, Wind loading of structures, CRC press, 2018.

[9] D. Li, B. Liu, X. Zhou, Z. Wang, Size effects of area extreme pressure for large-scale cladding, in: Structures, volume 29, Elsevier, 2021, pp. 408–415.

[10] J. Wacker, R. Friedrich, E. Plate, U. Bergdolt, Fluctuating wind load on cladding elements and roof pavers, Journal of Wind Engineering and Industrial Aerodynamics 38 (1991) 405–418. URL: https://www.sciencedirect.com/science/article/pii/0167610591900585. doi:https://doi.org/10.1016/0167-6105(91)90058-5.

[11] E. Gavanski, Y. Uematsu, Local wind pressures acting on walls of low-rise buildings and comparisons to the japanese and us wind loading provisions, Journal of Wind Engineering and Industrial Aerodynamics 132 (2014) 77–91.

[12] X. Peng, L. Yang, E. Gavanski, K. Gurley, D. Prevatt, A comparison of methods to estimate peak wind loads on buildings, Journal of Wind Engineering and Industrial Aerodynamics 126 (2014) 11–23.

[13] D. Banks, R. Meroney, P. Sarkar, Z. Zhao, F. Wu, Flow visualization of conical vortices on flat roofs with simultaneous surface pressure measurement, Journal of Wind Engineering and Industrial Aerodynamics 84 (2000) 65–85.

[14] J.-X. Lin, D. Surry, H. Tieleman, The distribution of pressure near roof corners of flat roof low buildings, Journal of wind engineering and industrial aerodynamics 56 (1995) 235–265.

[15] J. Lin, D. Surry, The variation of peak loads with tributary area near corners on flat low building roofs, Journal of Wind Engineering and Industrial Aerodynamics 77 (1998) 185–196.

[16] L. Amerio, G. Lamberti, G. Pomaranzi, A. Zasso, C. Gorlé, Comparison of high-resolution pressure peaks in closed and open-section wind tunnels, in: Conference of the Italian Association for Wind Engineering, Springer, 2018, pp. 35–48.

[17] G. Lamberti, L. Amerio, G. Pomaranzi, A. Zasso, C. Gorlé, Comparison of high resolution pressure measurements on a high-rise building in a closed and open-section wind tunnel, Journal of Wind Engineering and Industrial Aerodynamics 204 (2020) 104247. URL: http://www.sciencedirect.com/science/article/pii/S0167610520301574. doi:https://doi.org/10.1016/j.jweia.2020.104247.

[18] M. Asghari Mooneghi, P. Irwin, A. Gan Chowdhury, Partial turbulence simulation method for predicting peak wind loads on small structures and building appurtenances, Journal of Wind Engineering and Industrial Aerodynamics 157 (2016) 47–62. URL: https://www.sciencedirect.com/science/article/pii/S0167610516304202. doi:https://doi.org/10.1016/j.jweia.2016.08.003.

[19] H. Tieleman, R. Akins, Effects of incident turbulence on pressure distributions on rectangular prisms, Journal of Wind Engineering and Industrial Aerodynamics 36 (1990) 579–588.

[20] C. Farell, A. K. Iyengar, Experiments on the wind tunnel simulation of atmospheric boundary layers, Journal of wind engineering and industrial aerodynamics 79 (1999) 11–35.

[21] R. I. Harris, Ximis, a penultimate extreme value method suitable for all types of wind climate, Journal of Wind Engineering and Industrial Aerodynamics 97 (2009) 271–286.

[22] E. Gavanski, N. J. Cook, Evaluation of ximis for assessing extreme pressure coefficients, Frontiers in Built Environment 5 (2019) 48.

[23] J. L. Hintze, R. D. Nelson, Violin plots: a box plot-density trace synergism, The American Statistician 52 (1998) 181–184.

[24] Violin plot — Wikipedia, the free encyclopedia, 2021. URL: https://en.wikipedia.org/wiki/Violin_plot.